AGU PUBLICATIONS

JGR

Journal of Geophysical Research: Solid Earth

RESEARCH ARTICLE
10.1002/2017JB014950

Key Points:
- We implement the W-phase algorithm at regional scale to conduct real-time rapid source inversions in China and nearby area
- With minor modifications to the W-phase algorithm, reliable source parameters are obtained within 4 to 7 min after origin time
- Regional W-phase inversion can provide accurate results not only for large earthquakes but also for small events down to M_w = 5.0

Supporting Information:
- Supporting Information S1

Correspondence to:
X. Zhao,
zhaox@mail.iggcas.ac.cn

Citation:
Zhao, X., Duputel, Z., & Yao, Z. (2017). Regional W-phase source inversion for moderate to large earthquakes in China and neighboring areas. *Journal of Geophysical Research: Solid Earth*, *122*. https://doi.org/10.1002/2017JB014950

Received 3 SEP 2017
Accepted 21 NOV 2017
Accepted article online 24 NOV 2017

Regional W-Phase Source Inversion for Moderate to Large Earthquakes in China and Neighboring Areas

Xu Zhao[1], Zacharie Duputel[2], and Zhenxing Yao[1]

[1]Key Laboratory of Earth and Planetary Physics, Institute of Geology and Geophysics, Chinese Academy of Sciences, Beijing, China, [2]Institut de Physique du Globe de Strasbourg, UMR7516, Université de Strasbourg/EOST, CNRS, Strasbourg, France

Abstract Earthquake source characterization has been significantly speeded up in the last decade with the development of rapid inversion techniques in seismology. Among these techniques, the W-phase source inversion method quickly provides point source parameters of large earthquakes using very long period seismic waves recorded at teleseismic distances. Although the W-phase method was initially developed to work at global scale (within 20 to 30 min after the origin time), faster results can be obtained when seismological data are available at regional distances (i.e., $\Delta \leq 12°$). In this study, we assess the use and reliability of regional W-phase source estimates in China and neighboring areas. Our implementation uses broadband records from the Chinese network supplemented by global seismological stations installed in the region. Using this data set and minor modifications to the W-phase algorithm, we show that reliable solutions can be retrieved automatically within 4 to 7 min after the earthquake origin time. Moreover, the method yields stable results down to M_w = 5.0 events, which is well below the size of earthquakes that are rapidly characterized using W-phase inversions at teleseismic distances.

1. Introduction

Fast earthquake source characterization provides key information that can subsequently be used for tsunami warning, rapid damage assessment, and planning of rescue operations. In this context, rapid centroid moment tensor (CMT) inversion provides essential parameters that directly outline the size, geometry, and kinematic properties of the rupture (i.e., magnitude, focal mechanism, and duration). Such parameters can in turn be used to rapidly assess tsunami wave heights (Wang et al., 2012) and ground motion amplitude (Dreger et al., 2005).

Rapid earthquake source inversion is a challenging problem for multiple reasons. First, the size and complexity of large ruptures generate complicated waveforms that are difficult to model at periods shorter than 100 s. Second, the uneven distribution of seismic networks, malfunctioning stations, and noisy records are troublesome to handle automatically. To cope with the difficulty to rapidly characterize the source of large earthquakes, Kanamori and Rivera (2008a) proposed to perform CMT inversions using the W-phase, a long period signal corresponding to the superposition of the first overtones of normal modes at periods longer than 100 s (Kanamori, 1993). The W-phase algorithm was primarily developed to rapidly retrieve the source properties of $M_w \geq 7.5$ earthquakes within 20–35 min after the event origin time using teleseismic records at epicentral distances $\Delta \leq 90°$. This approach provides robust results for $M_w \geq 6.0$ earthquakes (Duputel et al., 2012) and has thus been implemented in various agencies and tsunami warning centers (Duputel et al., 2011; Hayes et al., 2009).

Although the W-phase algorithm yields essential information for large-scale earthquake response, getting faster solutions is desirable since a 20 min delay is often not fast enough for regional tsunami warning and rescue operations. The computational time being negligible, the delay of availability of the results is determined by the travel time of the W-phase. Source inversion results can thus be speeded up using broadband seismograms at shorter distances (i.e., using stations within $\Delta \leq 12°$). This can only be achieved when sufficiently good station coverage is available at regional scale. Using this approach, Kanamori and Rivera (2008b) and Duputel et al. (2011) demonstrated that faster W-phase solutions can be obtained using dense Japanese broadband data. Such regional implementations can also benefit from high-rate GPS data as shown by Rivera et al. (2011) in Japan and by Riquelme et al. (2016) in Chile.

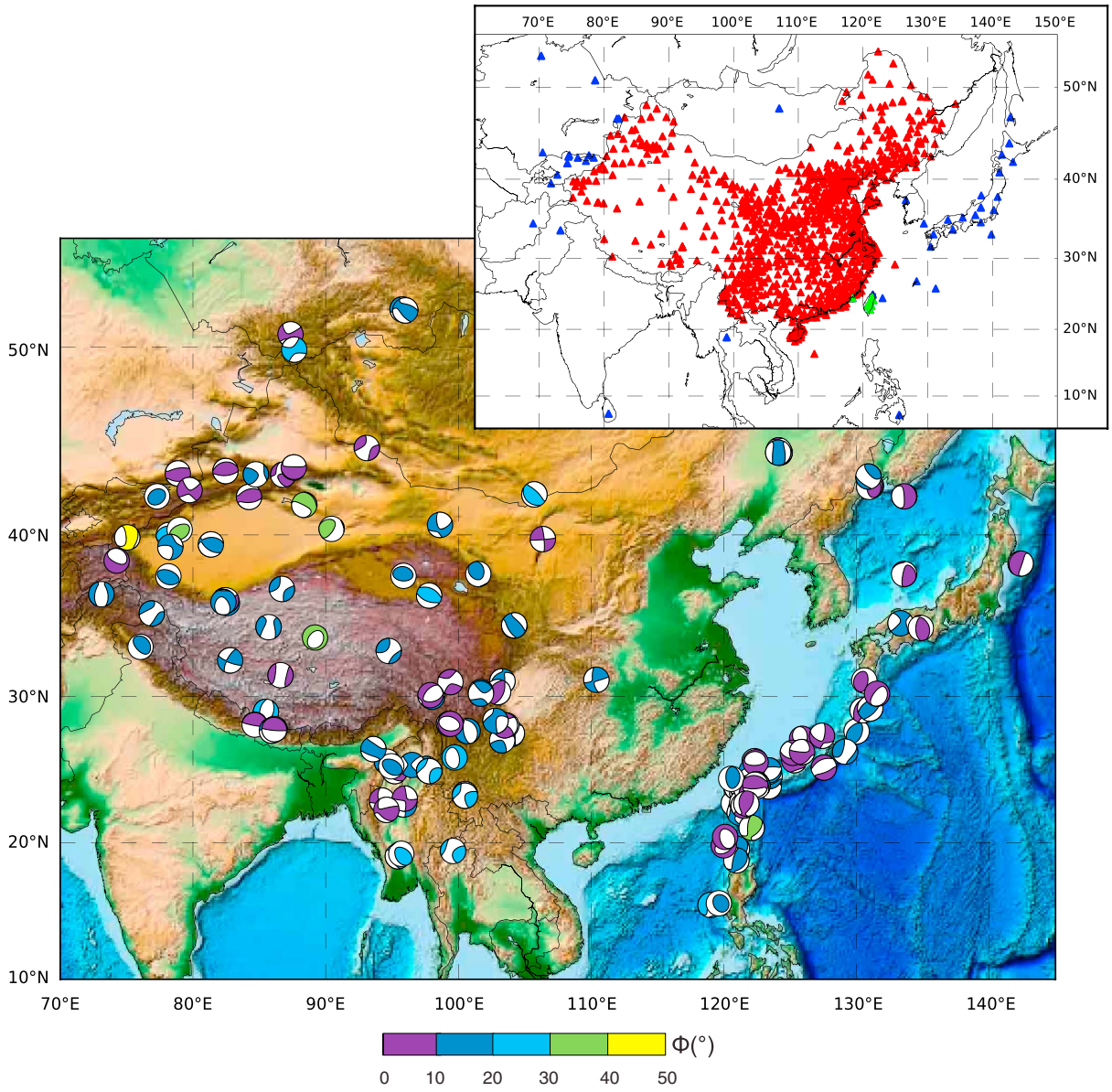

Figure 1. W-phase solutions obtained for $M \geq 5.0$ earthquakes. Studied events include $M \geq 5.0$ events in China and neighboring areas from November 2011 to November 2015 along with the 2008 $M_w = 7.9$ Wenchuan earthquake and the 2011 $M_w = 9.1$ Tohoku earthquake. Beach balls are colored according to the angular difference Φ with respect to the Global Centroid-Moment Tensor (GCMT) solution (see equation (3) in the main text). These solutions were obtained using stations presented in the upper right inset using red, green, and blue triangles for China, Taiwan, and global networks, respectively.

In this study, we implement the W-phase algorithm at regional scale to rapidly characterize the source of moderate to large ($M_w \geq 5.0$) earthquakes in China and neighboring areas. China is one of the most active seismic regions in the world and is currently experiencing a notable increase in the number of seismological stations (Figure 1). Using real-time data streams from about 974 permanent seismic stations, the China Earthquake Networks Center (CENC) is now able to rapidly provide preliminary hypocenter location, origin time, and magnitude. The purpose of this work is to evaluate the accuracy and rapidity of the W-phase approach using regional data and the preliminary earthquake information provided by the CENC. To this end, we analyze the CMT parameters that are inverted automatically for $M \geq 5.0$ earthquakes in China and neighboring areas between 2011 and 2015 (145 events). We also evaluate the performance of the W-phase algorithm for the 2008 $M_w = 7.9$ Wenchuan earthquake and the 2011 $M_w = 9.1$ Tohoku event. We further

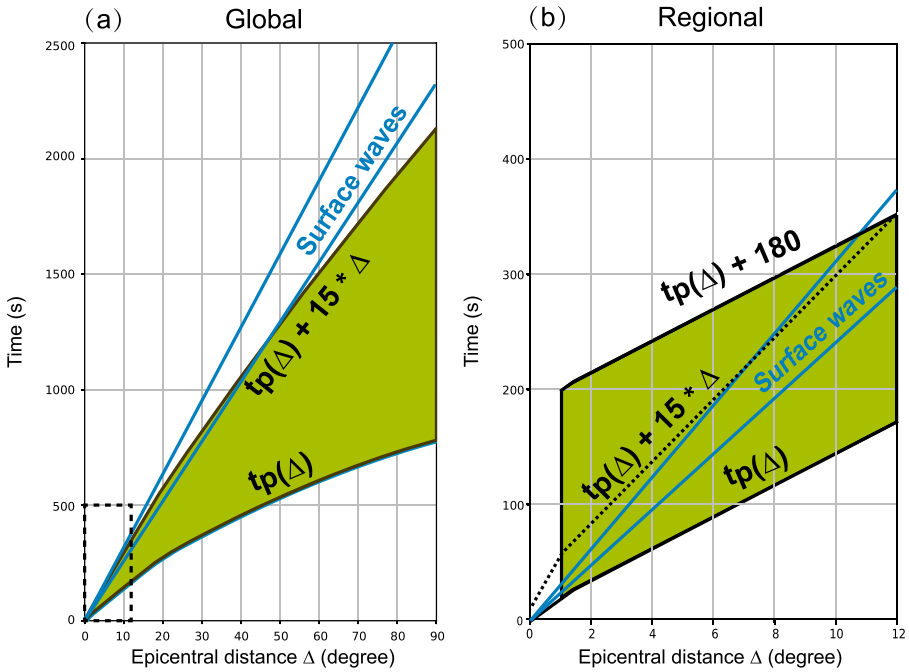

Figure 2. W-phase time windows for (a) global and (b) regional applications. Green areas indicate the portion of the records that are selected for inversion. $t_p(\Delta)$ shows the *P* wave arrival time for different epicentral distances Δ.

discuss the effects of the maximum epicentral distance, time window length, and velocity model on the accuracy of inverted results.

2. Data and Method

2.1. Data Selection and Processing

Our data set includes broadband records from more than 970 seismic stations retrieved at the CENC in real time (Figure 1). To improve the station coverage in neighboring regions, we also incorporate real-time data streams from Taiwan and global seismological networks (green and blue triangles, respectively, in Figure 1).

A key point to ensure the robustness of real-time W-phase solutions is the selection of stations providing high-quality data at long period. More specifically, we have to exclude noisy records associated with incorrect instrument responses or stations that are not adapted to the recording of long period seismic waves. For this purpose, we have manually defined an optimum set of stations by systematically comparing long-period observations and point source synthetic waveforms for several large teleseismic earthquakes. Using this procedure, we selected 825 stations providing high-quality waveforms at long period. This preliminary data selection is complemented by an automated data screening procedure in which noisy records are discarded before inversion (Duputel et al., 2012). In China, the selected stations are generally those equipped with BBVS-120, CTS-1, CMG-3ESPC, JCZ-1, JCZ-1T STS-1, and STS-2 instruments, while other international stations are with mainly STS-1 and STS-2 sensors.

Defining appropriate time window for the inversion is essential because it dictates both the delay in availability of the results and the amount of data used for the inversion. At a given epicentral distance Δ, the W-phase waveforms are generally selected from the *P* arrival time $t_p(\Delta)$ until $t_p(\Delta) + 15\ \text{s deg}^{-1} \times \Delta$ (Kanamori & Rivera, 2008a). This definition is appropriate for global application but yields very short waveforms at regional distances (Figure 2). Following Kanamori and Rivera (2008b), we thus extend the W-phase time window to $t_p(\Delta) + 180$ s at distances $\Delta \leq 12°$ (Figure 2b). Although the inversion is conducted using the same procedure as global W-phase inversions, a portion of the surface wave trains are incorporated in the inverted time window.

Table 1
Corner Frequency Bands Used for Band-Pass Filtering

Moment magnitude, M_w	Frequency band, mHz (s)
$M_w \geq 8.0$	1.0–5.0 (200–1,000)
$8.0 > M_w \geq 7.5$	1.7–6.7 (150–600)
$7.5 > M_w \geq 7.0$	2.0–8.3 (120–500)
$7.0 > M_w \geq 6.5$	4.0–10.0 (100–250)
$6.5 > M_w$	6.7–20.0 (50–150)

To maximize the signal to noise ratio for a wide range of magnitudes, we automatically adapt the passband corner frequencies given the preliminary magnitude provided by the CENC. For $M_w \geq 8.0$ earthquakes, we filter the waveforms within the standard W-phase frequency band 1–5 mHz (Kanamori & Rivera, 2008a). For smaller earthquakes ($5.0 \leq M_w < 8.0$), we gradually increase corner frequencies to reduce long-period noise in the records (Duputel et al., 2012; Hayes et al., 2009).

2.2. Regional W-Phase Method

Using the same procedure as Duputel et al. (2012), we invert for the full set of CMT parameters, including the moment tensor, the centroid location (latitude, longitude, and depth) and the centroid time. We also assume a triangular moment rate function with a half duration identical to the centroid delay (i.e., the delay between the origin time and the centroid time).

Real-time W-phase inversions at the CENC involve three main stages. First, the inversion assumes a centroid location fixed at the preliminary epicenter determined by the CENC automated system. The preliminary magnitude issued at the CENC is also used to obtain a preliminary estimate of the centroid time delay (Duputel et al., 2012) and to define the passband used to filter the waveforms (Table 1). To avoid any artifact due to an incorrect preliminary magnitude, the frequency passband is further updated using the scalar moment estimated after a first W-phase inversion. In the second stage, we perform a grid search to estimate the optimum centroid time delay minimizing the root-mean-square (RMS) of the waveform misfit. Finally, we perform another grid search to estimate the optimum centroid location, which yields our final centroid moment tensor solution. The employed grid search procedure is detailed in Duputel et al. (2012).

To speed up the inversion process, grid searches performed in the second and last stages are parallelized using OpenMP. Our data set comprising several thousands of records, we also use a parallel procedure to deal with data processing (instrument correction, waveform filtering, etc.). The full CMT inversion including the data preparation is usually computed in less than 30 s using 12 Xeon X5690 CPU cores.

3. Automated W-Phase CMT Inversions From 2011 to 2015

Of 153 events with $M \geq 5.0$ in the CENC catalog from November 2011 to November 2015 (available at http://data.earthquake.cn, last accessed May 2017), 145 events also had solutions in the GCMT catalog (http://www.globalcmt.org/CMTsearch.html; Dziewonski et al., 1992; Ekström et al., 2012), making them suitable to assess the reliability of W-phase solutions. To better evaluate the performance of our implementation for very large earthquakes, we also performed W-phase inversions for the 2011 M_w = 9.1 Tohoku and the 2008 M_w = 7.8 Wenchuan earthquakes. Events that occurred before August 2013 were used to tune the W-phase algorithm for automated operations in China (i.e., to define appropriate frequency passbands, data screening parameters, and time window). The solutions obtained after August 2013 were inverted in real time using the resulting automated W-phase algorithm. Two W-phase inversions are conducted in a completely automated manner: (1) a first inversion using data within an epicentral distance $\Delta \leq 5°$ available 4 min after the origin time and (2) a second inversion 3 min later using stations within $\Delta \leq 12°$. In order to provide stable results, we established a minimum number of 10 channels to perform a W-phase inversion. In addition, the third stage of the inversion (i.e., the centroid location grid search) is conducted only if the station coverage is sufficient to ensure a stable solution (number of channel $N \geq 15$ and azimuthal gap $\gamma \leq 270°$).

3.1. First W-Phase Inversion Results: T_0 + 4 min ($\Delta \leq 5°$)

W-phase CMT solutions obtained 4 min after the origin time (i.e., using stations within $\Delta \leq 5°$) are shown in Figure 3 and from Figures S1 to S4 in the supporting information. Out of 145 earthquakes, we obtain stable solutions for 105 events with estimated magnitudes within ±0.2 units of the GCMT moment magnitude. On the other hand, 40 inversions were considered of low quality as a result of the poor station coverage (less than 10 channels remaining after data screening). Most of these events correspond to earthquakes occurring in poorly covered regions such as in western China. These low-quality solutions also incorporate some large earthquakes that are affected by the clipping of records at short epicentral distances (i.e., within $\Delta \leq 5°$), as noted in previous regional implementations (e.g., Kanamori & Rivera, 2008b). As discussed in section 4.2,

Figure 3. W-phase moment tensor solutions for $M_w \geq 5.8$ in China and neighboring area from November 2011 to November 2015 along with the 2011 $M_w = 9.1$ Tohoku and the 2008 $M_w = 7.8$ Wenchuan earthquakes. The events obtained for smaller magnitudes are presented in Figures S2–S4. The solutions are displayed in order of decreasing GCMT magnitude. *N* is the number of used channels after inversion, and γ is the azimuthal gap (in degrees). GCMT solutions are presented in green, W-phase solutions ($\Delta \leq 5°$) are shown in red, and W-phase solutions($\Delta \leq 12°$) are denoted in purple red. Note that automated W-phase inversions are only conducted when at least 10 channels are available after data screening (cf. section 3).

those events can actually be processed in less than 5 min if we remove stations at very short epicentral distances. Those undetermined events put aside, the majority of earthquakes are characterized accurately. As shown in Table 2 and Figure S1, all W-phase inversions provide magnitudes that are within ±0.2 units of the GCMT estimates.

Table 2
Statistical Comparison of W-Phase and Global CMT Solutions Using Stations Within $\Delta \leq 5°$ and $\Delta \leq 12°$

Distance	Event number	(ΔM_w)	RMS (ΔM_w)	p ($\lvert \Delta M_w \rvert \leq 0.1$)	p ($\lvert \Delta M_w \rvert \leq 0.2$)	(Φ)	RMS (Φ)	p ($\Phi \leq 20°$)	p ($\Phi \leq 30°$)
$\Delta \leq 5°$	106	0.02	0.06	90%	100%	14.4 °	16.9°	77%	95%
$\Delta \leq 12°$	147	0.01	0.06	92%	100%	13.0 °	15.5°	85%	96%

Note. The number of solutions obtained is indicated in each case (event number) along with the mean and RMS values of the magnitude difference ($\Delta M_w = M_w - M_{w-\mathrm{GCMT}}$) and focal mechanism angular difference (Φ). We also present the proportion (p) of solutions with $\Delta M_w \leq 0.1$, $\Delta M_w \leq 0.2$, $\Phi \leq 20°$, or $\Phi \leq 30°$.

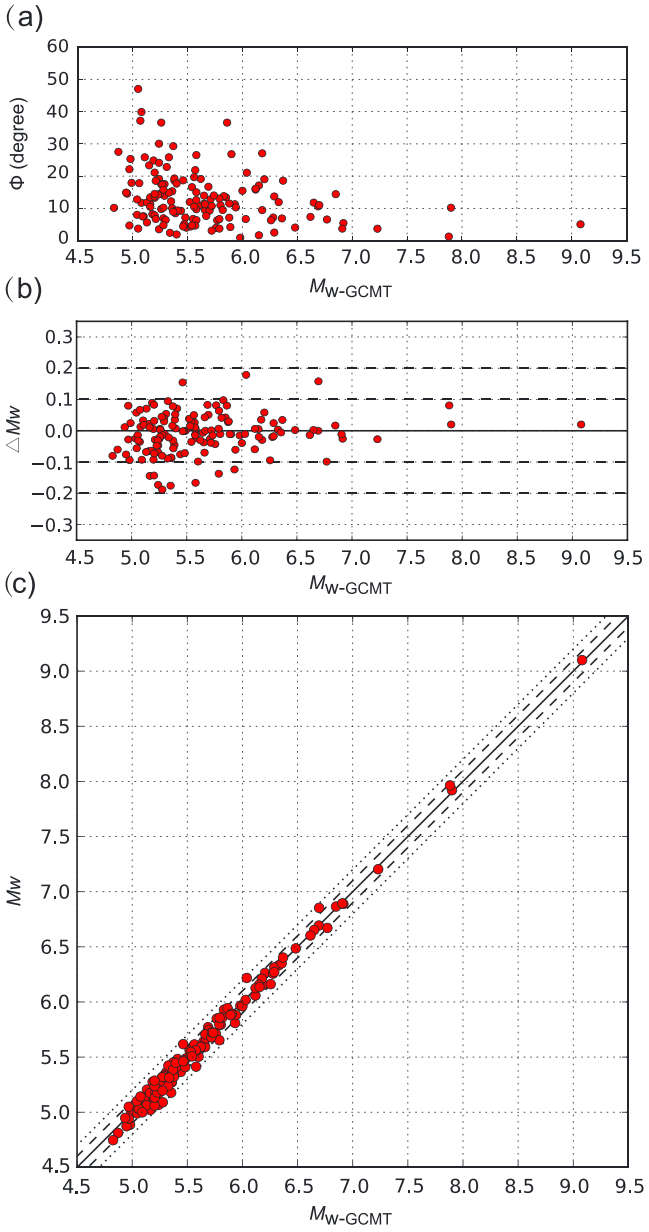

Figure 4. Comparison of W-phase and GCMT solutions obtained at T_0 + 7 min ($\Delta \leq 12°$). (a) Comparison between W-phase and GCMT focal mechanisms. Φ is the angular difference between W-phase and GCMT focal mechanisms (see equation (3)). (b) Magnitude difference $\Delta M_w = M_w - M_{w-\mathrm{GCMT}}$ between W-phase magnitude (M_w) and GCMT magnitude ($M_{w\ -\ \mathrm{GCMT}}$). (c) Comparison between W-phase (M_w) and GCMT magnitude ($M_{w-\mathrm{GCMT}}$).

To quantitatively compare W-phase and GCMT focal mechanisms, we also measure the difference of *P* or *S* radiation pattern (see Rivera & Kanamori, 2014)

$$\Delta_R = \frac{1}{2\sqrt{2}}\left[\left(\hat{\mathbf{M}}_{\mathbf{WCMT}} - \hat{\mathbf{M}}_{\mathbf{GCMT}}\right) : \left(\hat{\mathbf{M}}_{\mathbf{WCMT}} - \hat{\mathbf{M}}_{\mathbf{GCMT}}\right)\right]^{1/2} = \frac{1}{2\sqrt{2}}\left(\boldsymbol{D} : \boldsymbol{D}\right)^{1/2}. \quad (1)$$

where $\hat{\mathbf{M}}_{\mathbf{WCMT}}$ and $\hat{\mathbf{M}}_{\mathbf{GCMT}}$ are the normalized W-phase and GCMT moment tensors defined as $\hat{\mathbf{M}} = \boldsymbol{M}/\sqrt{\boldsymbol{M} : \boldsymbol{M}}$ with $\mathbf{M}$ the moment tensor and the double tensor contraction $\mathbf{M} : \mathbf{M} = M_{ij}M_{ij}$. $\boldsymbol{D}$ denotes the difference between $\hat{\mathbf{M}}_{\mathbf{WCMT}}$ and $\hat{\mathbf{M}}_{\mathbf{GCMT}}$. Explicitly expressed in terms of the components of $\boldsymbol{D}$, the above expression gives

$$\Delta_R = \frac{1}{2\sqrt{2}}\left(D_{11}^2 + D_{22}^2 + D_{33}^2 + 2\left(D_{12}^2 + D_{23}^2 + D_{31}^2\right)\right)^{1/2} \quad (2)$$

The angular difference Φ between W-phase and GCMT focal mechanisms is then defined as

$$\Phi = 2 \cdot \arcsin(\Delta_R) \quad (3)$$

For double-couple sources, this definition coincides with the geometrical angular distance between two focal spheres as defined by Kagan (1991). The resulting angular differences presented in Figure S1 and Table 2 indicate a relatively good agreement between GCMT and W-phase focal mechanisms with more than 95% of the solutions having $\Phi \leq 30°$ using stations within $\Delta \leq 5°$.

3.2. Second W-Phase Inversion Results: T_0 + 7 min ($\Delta \leq 12°$)

W-phase solutions obtained 7 min after origin time using stations within $\Delta \leq 12°$ are presented in Figures 1, 3, and Figures S2 to S4. In order to avoid the clipping issues noted in section 3.1, these solutions are obtained after removing all stations at distances shorter than 5°. Using this procedure, our regional implementation provides reliable results for the entire earthquake catalog considered in this study (i.e., $M_w \geq 5$ earthquakes). As shown in Figure 4 and Table 2, all solutions are within ±0.2 units of the GCMT moment magnitude and more than 90% of the events have a magnitude difference $\Delta M_w \leq 0.1$. W-phase focal mechanisms are also very stable with an angular difference $\Phi \leq 30°$ for 96% of the events (cf. Figure 1 and Table 2). However, as shown in Figure 4a, we notice that Φ increases for small magnitudes with an average value of $\langle\Phi\rangle \sim 15°$ for $M_w \leq 6$ and of $\langle\Phi\rangle \sim 10°$ for $M_w > 6$. This probably reflects a decrease of the signal-to-noise ratio for smaller magnitude earthquakes due to long period noise.

Figure 5 shows a comparison of W-phase and GCMT moment tensor estimates. Although the six elements of the moment tensor are in good agreement with GCMT, we notice a larger dispersion at small amplitude. This is probably related to the decrease of signal-to-noise ratio for small earthquakes as noted above. There is also a larger scatter for the moment tensor elements $M_{r\theta}$ and $M_{r\phi}$. These elements are more difficult to constrain for shallow earthquakes due to the small amplitude of the associated excitation kernels at long periods (Kanamori & Given, 1981). This results in a well-known trade-off between the dip angle δ and the scalar moment M_0 for shallow earthquakes (Tsai et al., 2011).

Figure 6 shows a comparison between W-phase and GCMT centroid locations. Overall, there is a relatively good agreement between both catalogs with an average great circle distance (ΔX) of 17 km and a depth

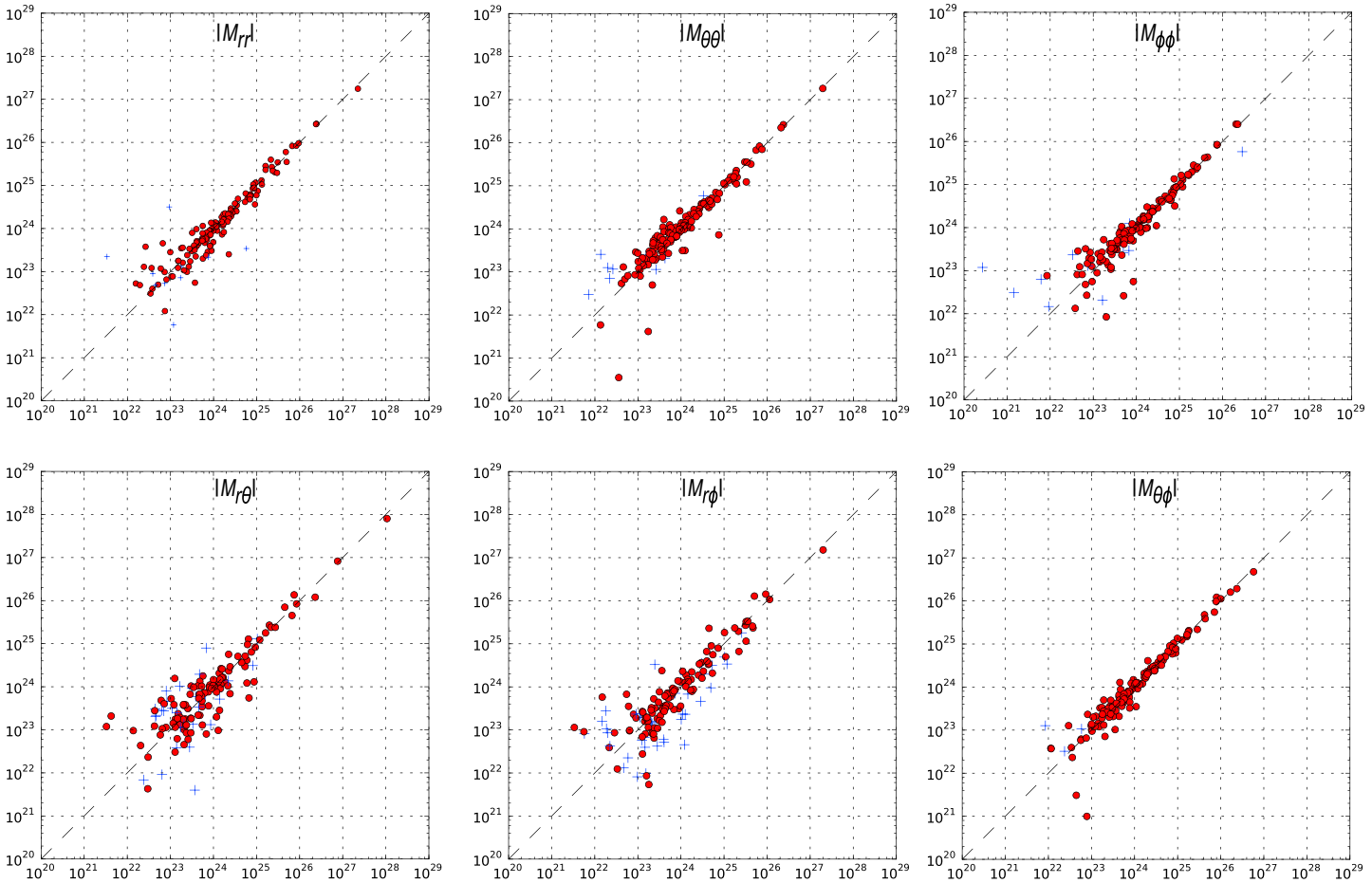

Figure 5. Comparisons of the moment tensor elements in dyne-cm of W-phase (vertical axis, unit: dyne-cm) and GCMT (horizontal axis, unit: dyne-cm) solutions. Red circles denote W-phase and GCMT moment tensor components having the same sign, and blue crosses denote opposite sign.

standard deviation of 8.5 km. The majority of events with $\Delta X \geq 30$ km are located in areas with sparse station coverage (e.g., central Tibet, northwestern Xinjiang, and Ryukyu Islands). There is no clear pattern in the orientation of mislocation vectors, except in Japan, Taiwan, and the Philippines where W-phase centroids seem to be biased toward the east. This is probably due to the unbalanced network geometry in these regions (i.e., large azimuthal gap), most stations being located in mainland China.

3.2.1. Example 1: 2011 M_w = 9.1 Tohoku Earthquake

Although the 2011 Tohoku earthquake is not included in our original catalog, this event is particularly valuable to evaluate the accuracy of our regional implementation for megathrust earthquakes. The W-phase solution obtained using data within $\Delta \leq 12°$ is presented in Figure 7. The results indicate that reliable source estimates can be determined using waveforms from regional seismic stations. The difference between M_w and $M_{w-\mathrm{GCMT}}$ is about 0.02, and the estimated thrust mechanism is consistent with the GCMT solution (angular difference Φ = 5.1°). We also notice that the optimal centroid time shift τ_{WCMT} = 67 s and centroid depth H_{WCMT} = 25 km are in good agreement with τ_{GCMT} = 70 s and H_{GCMT} = 20 km. The horizontal centroid location is shown in Figure 7c for the optimal centroid depth. W-phase and GCMT centroids are significantly different, with a horizontal distance ΔX~40 km. This mainly results from the unbalanced distribution of stations (azimuthal gap γ~180°). As illustrated in Figure 7, many records are clipped at short epicentral distances due to large amplitude surface waves. There are thus only a few stations available within $\Delta \leq 5°$. However, our tests show that a first reliable focal mechanism and moment magnitude (M_w = 9.03) can be obtained by including stations $\Delta \leq 6°$ and removing stations within $\Delta \leq 5°$ (Figure 7).

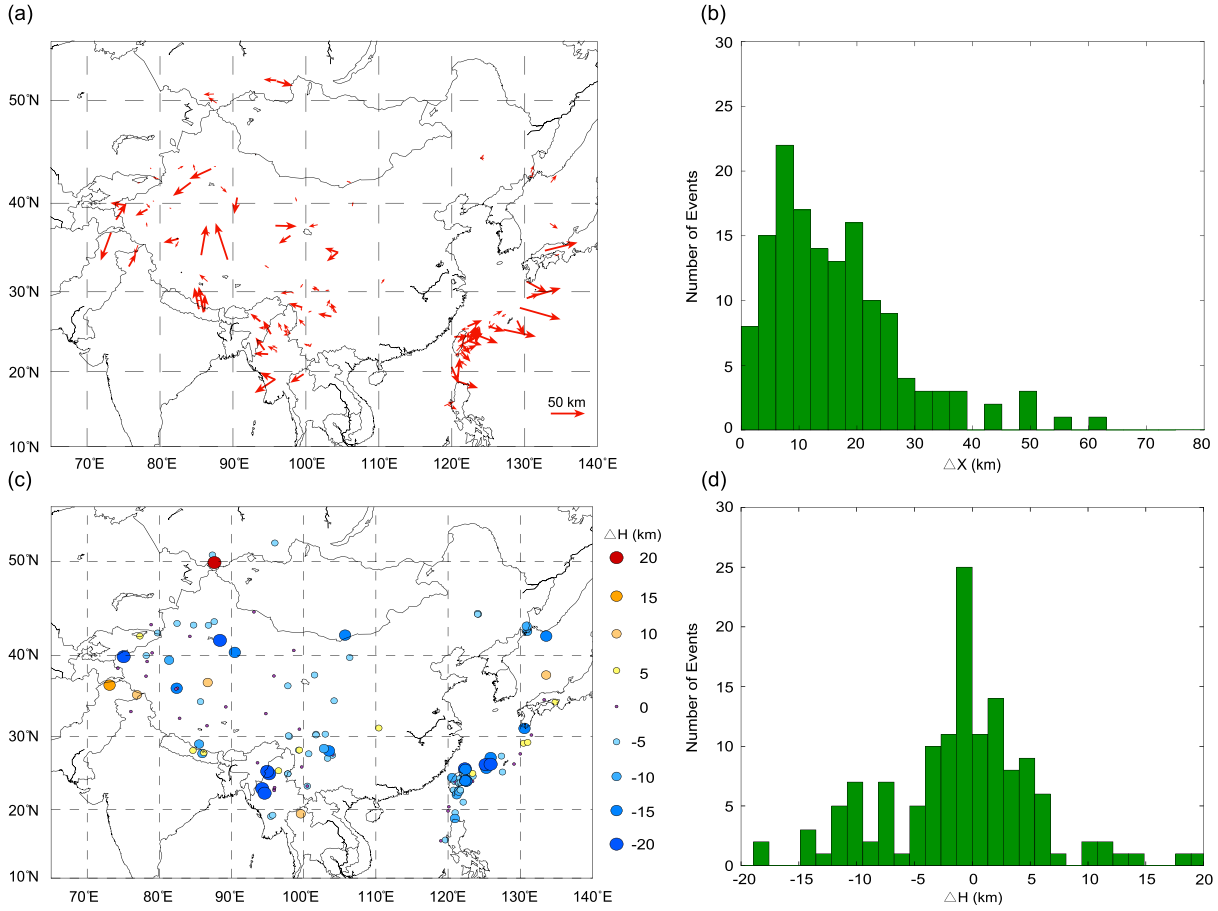

Figure 6. Comparison between W-phase and GCMT centroid locations. (a) Differences in locations. The arrows point from the GCMT to the W-phase centroid location. (b) Distribution of the great circle distance (ΔX) between W-phase and GCMT centroid locations. (c) Depth differences ($\Delta H = H_{\mathrm{WCMT}} - H_{\mathrm{GCMT}}$). (d) Distribution of ΔH.

3.2.2. Example 2: 2008 M_w = 7.9 Wenchuan Earthquake

The 2008 Wenchuan earthquake is the largest thrust event that occurred in continental China in the last 50 years. This event devastated cities along the northwest margin of the Sichuan basin, which caused more than 80,000 fatalities (Shen et al., 2009). Despite the clipping of records at short epicentral distances, results presented in Figure 8 indicate that W-phase solutions can be accurately determined using regional waveforms within $\Delta \leq 6°$ and $\Delta \leq 12°$. Figure 8a shows that automated W-phase solutions are in good agreement with the GCMT solution. Inversions performed at $\Delta \leq 6°$ and $\Delta \leq 12°$ provide reliable magnitude estimates (with a difference between $M_{w\text{-WCMT}}$ and $M_{w-\mathrm{GCMT}}$ of about 0.02) and focal mechanisms that are consistent with GCMT solutions (with an angular difference $\Phi \leq 11°$). These results show that the rupture is dominated by thrust motion with a minor strike-slip component, in agreement with previous studies (Shen et al., 2009; Wang et al., 2011; Xu et al., 2009). The optimal centroid time shift is about 34 s, which is similar to that from GCMT (39 s). As shown in Figure 8c, the horizontal location grid search yields a centroid that is located in the northeast of the epicenter. This is consistent with the northeastward rupture directivity that has been identified for this event (Parsons et al., 2008; Wang et al., 2008).

3.2.3. Example 3: 2015 M_w = 7.9 Gorkha Earthquake

The 25 April 2015 M_w = 7.9 Gorkha (Nepal) earthquake and its M_w = 7.2 aftershock are the first $M_w > 7.0$ events inverted in real time using our regional W-phase implementation at the CENC. Though the M_w = 7.9 Gorkha earthquake took place outside of our network, the W-phase solution was accurately determined in real time using waveforms from Chinese seismic stations within $\Delta \leq 12°$. The inversion results and the corresponding waveform fit are presented in Figure 9. Despite the clipping of records at multiple stations,

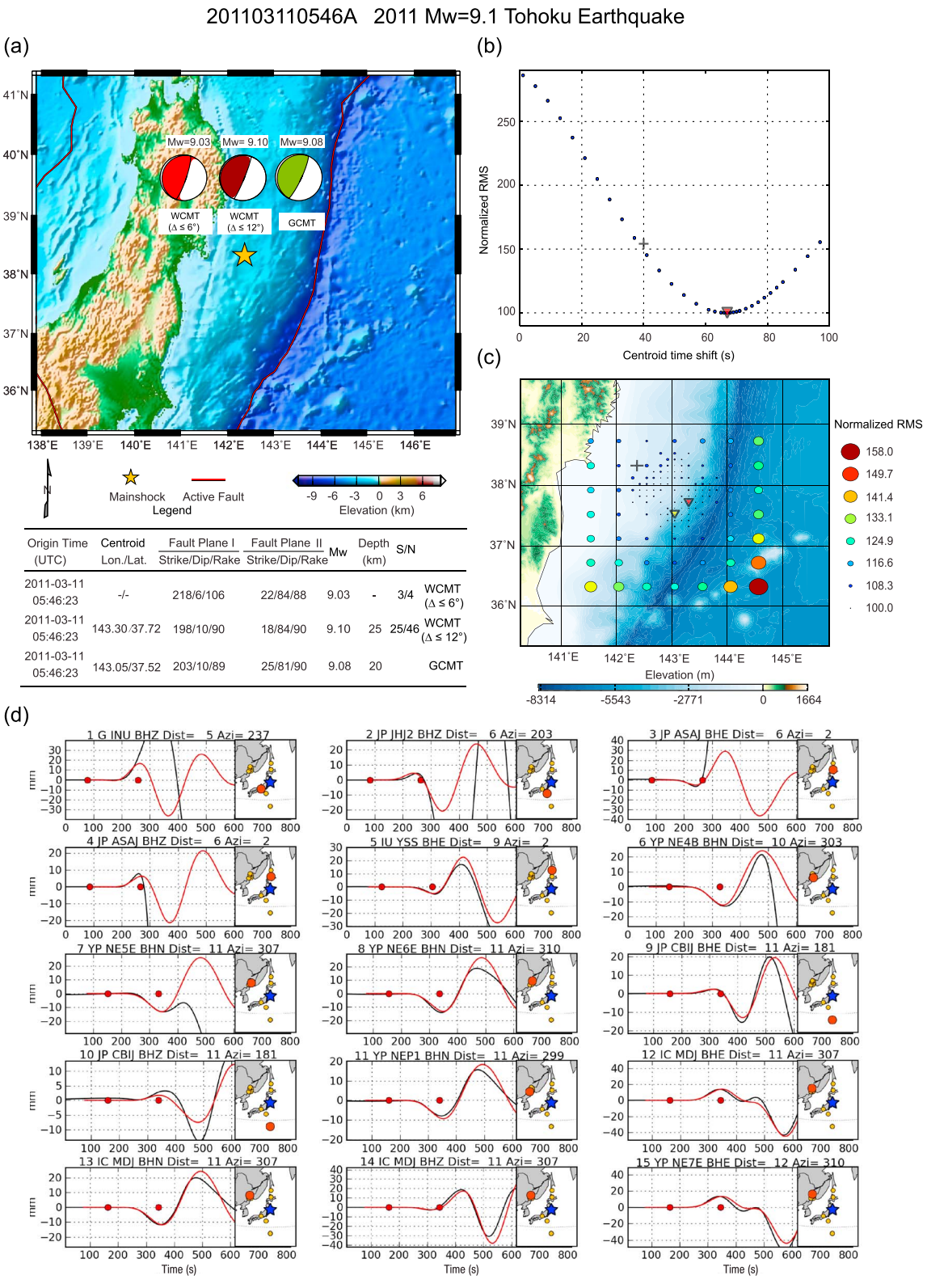

Origin Time (UTC)	Centroid Lon./Lat.	Fault Plane I Strike/Dip/Rake	Fault Plane II Strike/Dip/Rake	Mw	Depth (km)	S/N	
2011-03-11 05:46:23	-/-	218/6/106	22/84/88	9.03	-	3/4	WCMT (Δ ≤ 6°)
2011-03-11 05:46:23	143.30/37.72	198/10/90	18/84/90	9.10	25	25/46	WCMT (Δ ≤ 12°)
2011-03-11 05:46:23	143.05/37.52	203/10/89	25/81/90	9.08	20		GCMT

Figure 7. Regional W-phase inversion results for the 2011 M_w = 9.1 Tohoku earthquake. (a) Comparison of W-phase and GCMT solutions. *S* and *N* are the number of stations and channels, respectively. (b) Determination of the optimum centroid time shift obtained via grid search. (c) Centroid location grid search. The red and yellow triangles indicate the centroid horizontal location from W-phase and GCMT solutions, respectively. The black cross corresponds to the epicentral location determined by the CENC. (d) Comparison of observed (black) and predicted (red) waveforms for the solution obtained using stations within $\Delta \leq 12°$. Red circles indicate the selected time window for W-phase inversion. Network, station, channel, epicentral angular distance, and azimuth are indicated on top of each waveform.

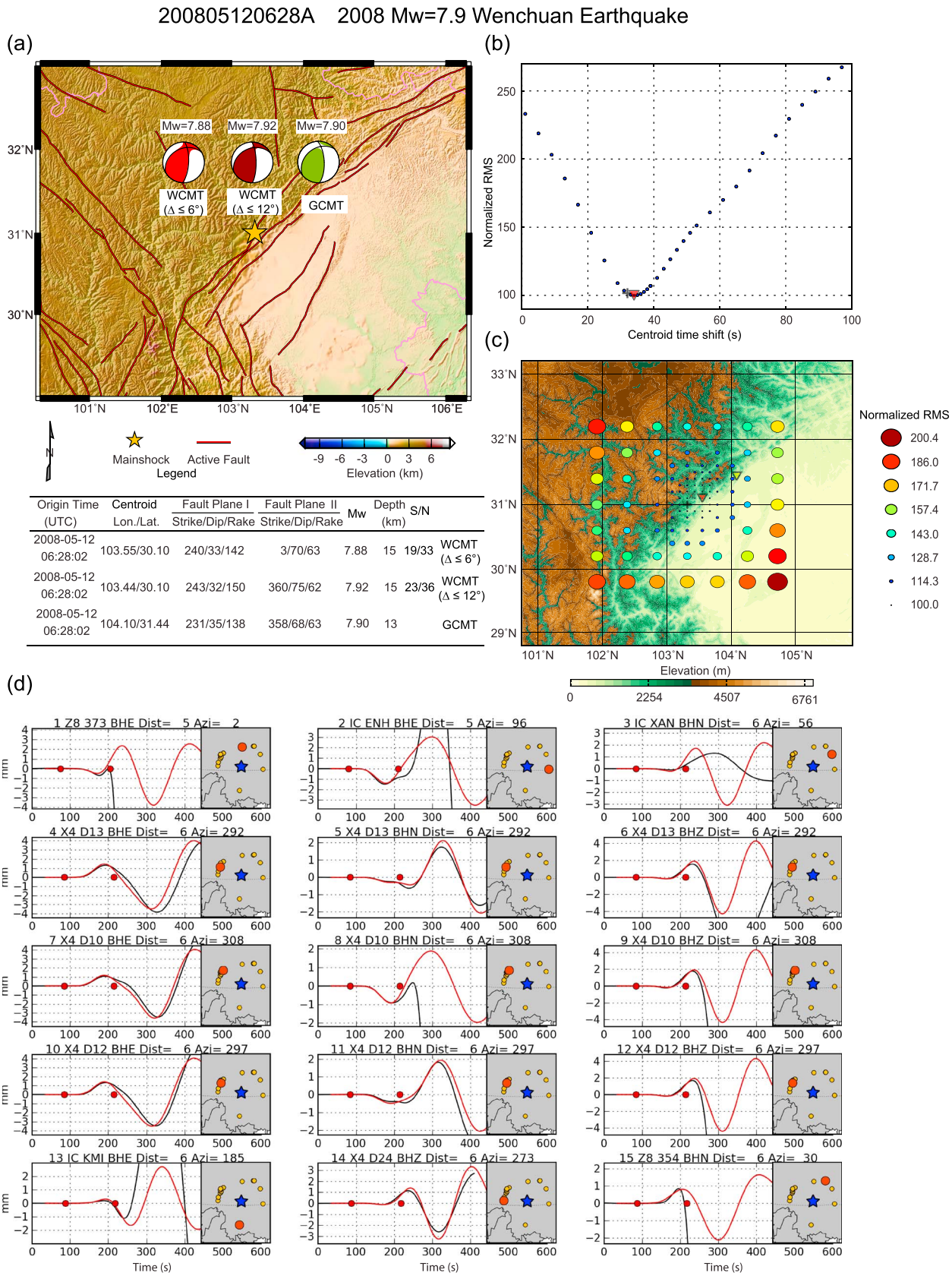

Origin Time (UTC)	Centroid Lon./Lat.	Fault Plane I Strike/Dip/Rake	Fault Plane II Strike/Dip/Rake	Mw	Depth (km)	S/N	
2008-05-12 06:28:02	103.55/30.10	240/33/142	3/70/63	7.88	15	19/33	WCMT (Δ ≤ 6°)
2008-05-12 06:28:02	103.44/30.10	243/32/150	360/75/62	7.92	15	23/36	WCMT (Δ ≤ 12°)
2008-05-12 06:28:02	104.10/31.44	231/35/138	358/68/63	7.90	13		GCMT

Figure 8. Regional W-phase inversion results for the 2008 M_w = 7.9 Wenchuan earthquake. Same as in Figure 7.

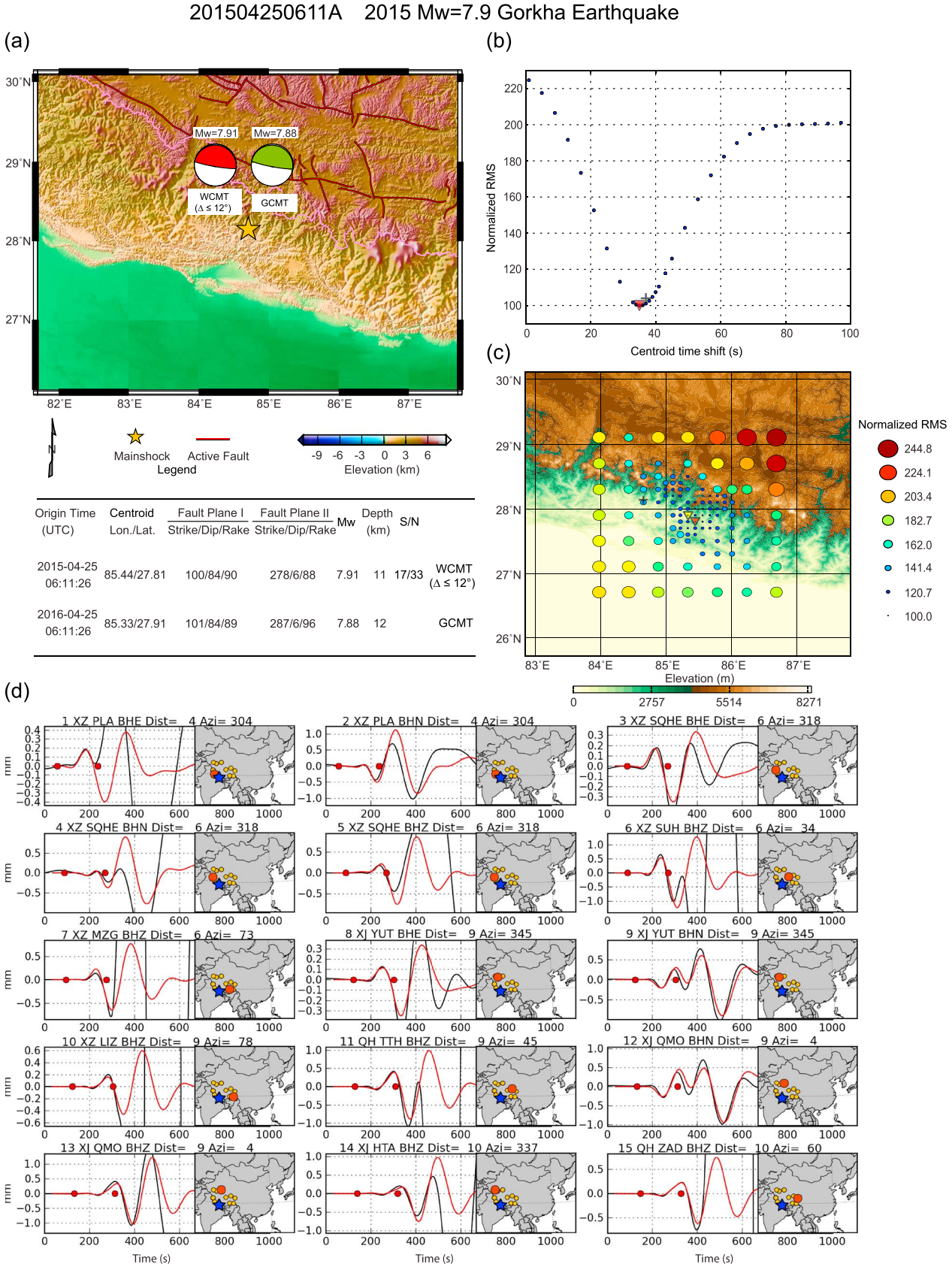

Figure 9. Regional W-phase inversion results for the 2015 M_w = 7.9 Gorkha earthquake. Same as in Figure 7.

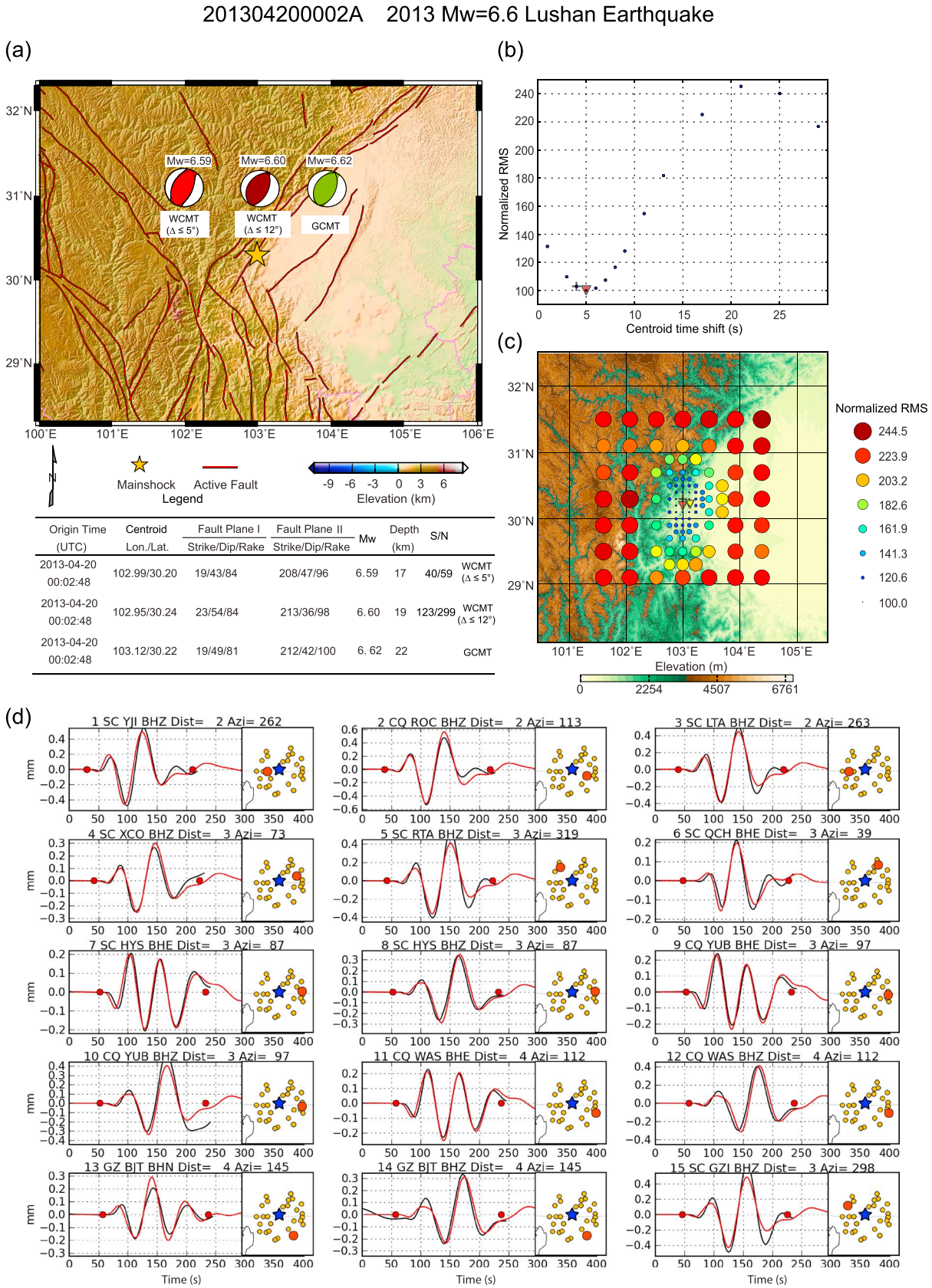

Figure 10. Regional W-phase inversion results for the 2013 M_w = 6.6 Lushan earthquake. Same as in Figure 7.

the W-phase waveforms are generally well recovered before the arrival of large amplitude seismic waves. The W-phase focal mechanism and moment magnitude are consistent with the GCMT solution, with a difference between $M_{w\text{-WCMT}}$ and $M_{w\text{-GCMT}}$ of only 0.03. As shown in Figure 9b, the optimal W-phase centroid time shift $\tau_{\text{WCMT}} = 35$ s also agrees with GCMT estimates $\tau_{\text{GCMT}} = 32$ s. Moreover, the W-phase point source is located in the southeast of the epicenter (cf. Figure 9c), which is consistent with the southeastward directivity of the rupture (e.g., Duputel et al., 2016; Yue et al., 2016).

3.2.4. Example 4: 2013 M_w = 6.6 Lushan Earthquake

The 20 April 2013 M_w = 6.6 Lushan earthquake occurred in Longmenshan (Sichuan, China), which is one of the most active regions of China. This event initiated about 84 km southwest of the 2008 Wenchuan earthquake epicenter. Given the density of seismic observations in the epicentral area, this event illustrates how rapidly a W-phase inversion can be performed in real time. As shown in Figure 10, the solutions obtained 4 min ($\Delta \leq 5°$) and 7 min ($\Delta \leq 12°$) after origin time are both within 0.03 magnitude unit of $M_{w\text{-GCMT}}$. W-phase focal mechanisms are consistent with GCMT with an angular difference smaller than 14° for both solutions. Centroid time shift and location are also consistent with GCMT estimates. The W-phase centroid location is located south of the CENC epicenter over the large-slip area inferred by Hao et al. (2013) and Zhao et al. (2014).

3.2.5. Example 5: 2013 M_w = 4.9 Jilin Earthquake

The 22 November 2013 M_w = 4.9 Jilin earthquake occurred in eastern China. It is an interesting example to illustrate the ability of our regional implementation to retrieve source parameters of small earthquakes ($M_w \leq 6.0$). Because of the availability of numerous stations in the epicenter area, W-phase solutions can be obtained for this event using records within $\Delta \leq 5°$ and $\Delta \leq 12°$. As shown above for large earthquakes, the solutions presented in Figure 11 are in good agreement with the GCMT solution. The difference between $M_{w\text{-WCMT}}$ and $M_{w\text{-GCMT}}$ is about 0.12 when using data within $\Delta \leq 5°$ and is reduced to 0.03 when the data set is supplemented by stations at $\Delta \leq 12°$. W-phase focal mechanisms are remarkably similar to GCMT with an angular difference $\Phi \leq 13°$. The optimum centroid time shift is 1 s, consistent with that from GCMT (0.7 s), and the centroid mislocation is smaller than 5 km. This demonstrates that W-phase solutions for M_w = 5.0 earthquakes can be accurately determined using our regional W-phase implementation.

4. Discussion

4.1. Accuracy of Regional W-Phase Solutions

Rapid CMT inversion is a central part of ongoing efforts at the CENC to improve the fast characterization of earthquakes in China and neighboring areas. In this study, we show that rapid W-phase CMT solutions can be obtained in this region using broadband data from Chinese seismic networks. Reliable source parameters can be obtained for moderate to large earthquakes ($M_w \geq 6.0$) and also for lower magnitude events down to M_w = 5.0 with only minor modifications to the W-phase algorithm.

Within only 7 min after the origin time, reliable W-phase CMT solutions can be obtained for all $M_w \geq 5$ earthquakes in our catalog. This provides a significant speedup compared to the 20 to 35 min delay of teleseismic W-phase solutions. When sufficient data are available at very short epicentral distances ($\Delta \leq 5°$), this delay can be further reduced to 4 min. However, due to the poor station coverage in some regions or to the clipping of records for large earthquakes, the number of inverted channels is not always sufficient to yield a stable W-phase solution in 4 min only. In the future, such limitations could be avoided by incorporating high-rate GPS data that is not subject to clipping and proved effective in other regional applications (e.g., Riquelme et al., 2016; Rivera et al., 2011). It is worth noting that the W-phase approach often performs relatively well with a small set of waveforms ($N \leq 15$ or $\gamma \leq 270°$), such as for the 2011 M_w = 9.1 Tohoku Earthquake and the 2008 M_w = 7.9 Wenchuan earthquake. Nevertheless, even if accurate moment tensor parameters can be estimated using a limited number of waveforms, good station coverage is crucial to obtain a reliable centroid location.

4.2. Effects of Station Distance and Time Window Length

To further improve the current implementation, we tested the performance of the W-phase algorithm using different epicentral distances and time window lengths. Such tests are presented in Figure 12 for four events:

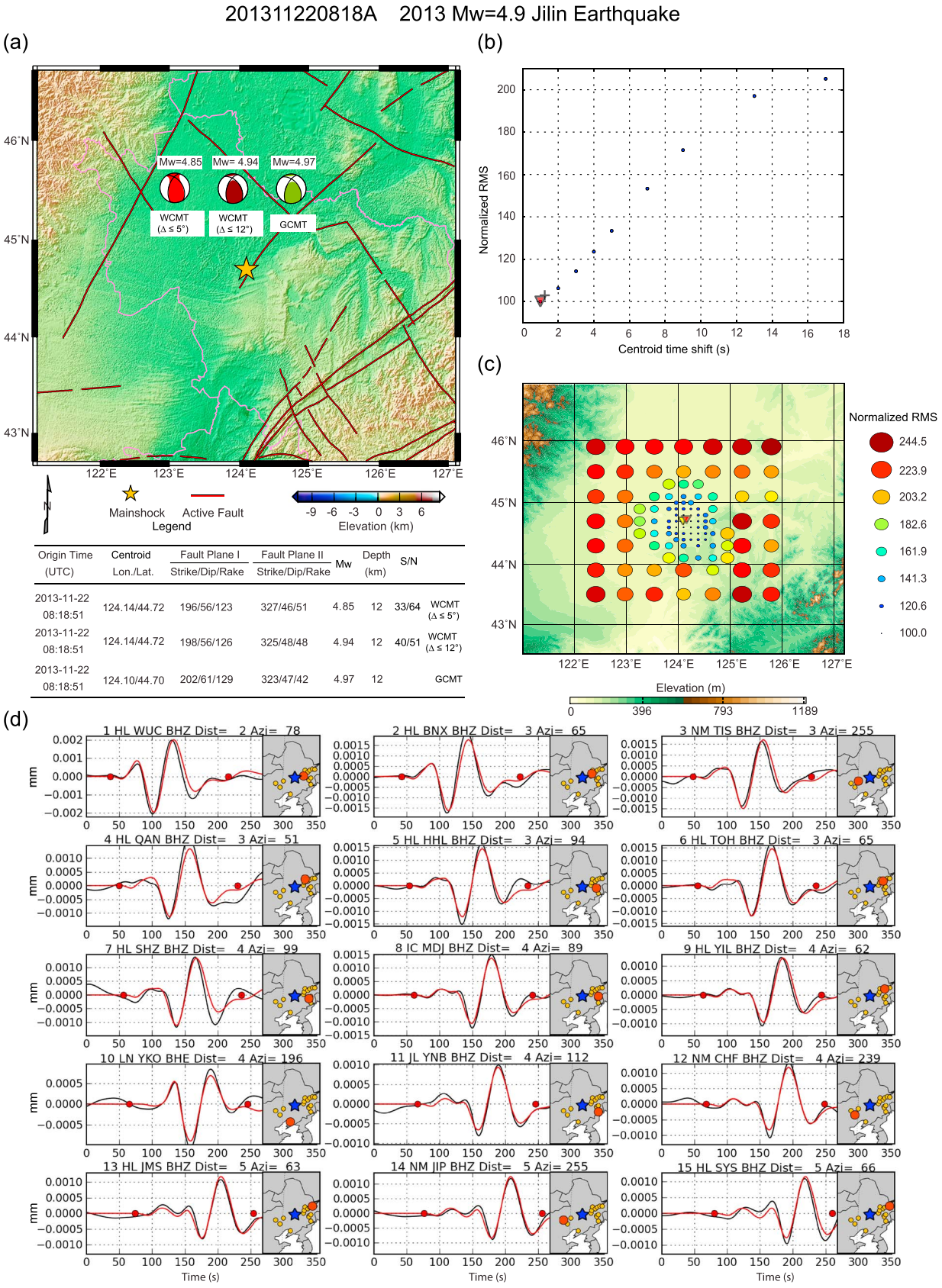

Figure 11. Regional W-phase inversion results for the 2013 M_w = 4.9 Jilin earthquake. Same as in Figure 7.

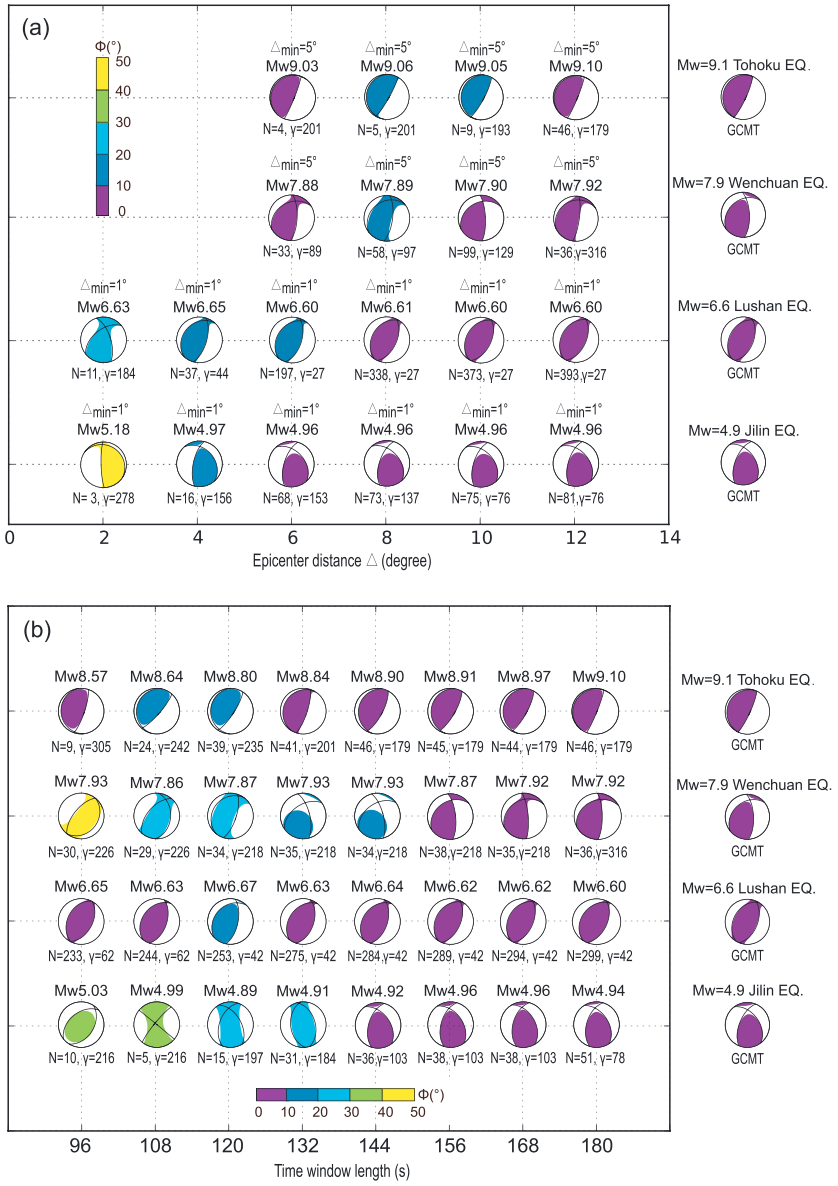

Figure 12. W-phase solutions obtained for four earthquakes using variable maximum (a) epicentral distance Δ and (b) time window length. In Figure 12a, the time window length is assumed to be 180 s. *N* is the channel number after inversion, and γ is the azimuthal gap (in degrees). In Figure 12b, we incorporate stations within $5° \leq \Delta \leq 12°$. Beach balls are colored based on the angular difference Φ with respect to GCMT solutions (see equation (3) in the main text).

the 2011 M_w = 9.1 Tohoku, the 2008 M_w = 7.9 Wenchuan, the 2013 M_w = 6.6 Lushan, and the 2013 M_w = 4.9 Jilin earthquakes.

Although W-phase solutions are better constrained when incorporating stations at larger epicentral distances, Figure 12a shows that faster reliable solutions can be obtained in 5 min by incorporating data within $\Delta \leq 6°$ of the epicenter and removing near-field stations for large earthquakes (to overcome limitations due to clipping issues and unaccounted finite-fault effects). To provide more reliable estimates, future implementations should thus adapt the minimum epicentral distance given the preliminary magnitude of the earthquake (using standard scaling relationships; e.g., Aki, 1967). Figure 12b also shows that W-phase solutions are relatively stable when reducing the time window length to 130 s. For future implementations, we could thus use narrower time windows to obtain faster solutions. However, the reduction of the time window length might

be problematic for great earthquakes that have very long rupture durations. For example, moment magnitude estimates for the 2011 M_w = 9.1 Tohoku earthquake are clearly underestimated when using a time window that is narrower than the total rupture duration (~170 s; Lee et al., 2011). This is probably due to the fact that the late part of the rupture is not captured using shorter time windows.

To assess the benefits of incorporating more observations, we also performed inversions extending our data set to stations within $\Delta \leq 20°$. The comparison of the resulting W-phase solutions with GCMT is presented in Figure S5 and Table S1 of the supporting information. There is no significant improvement of magnitude estimates that are already quite reliable using data within $\Delta \leq 12°$ (cf. Figure 4 and Table 2). However, we notice that W-phase focal mechanisms obtained at $\Delta \leq 20°$ are globally in better agreement with GCMT. This is clear in Figure S5 showing that nearly all solutions have an angular difference $\Phi \leq 30°$. Such results being available in about 10 min in real-time conditions, it might be interesting for future implementations to update W-phase solutions by incorporating stations up to $\Delta \leq 20°$.

4.3. Impact of the Elastic Structure

W-phase solutions presented above were obtained using Green's functions computed by the PREM model (Dziewonski & Anderson, 1981). To assess the possible benefits of using regional velocity models, we select four moderate-sized earthquakes in Yunnan where the dense broadband seismic network provides high-quality long-period records. We estimate W-phase CMT solutions for these four earthquakes using a regional 1-D velocity model presented in Figure S6. Green's functions are computed using Herrmann (2013) implementation of the wave number integration algorithm (Bouchon, 2003). Table S2 shows the comparison of inverted results with Global CMT solutions along with double-couple solutions obtained using the cut-and-paste (CAP) method (available at http://www.cea-igp.ac.cn; Zhao & Helmberger, 1994).

As presented in Table S2, W-phase solutions obtained using PREM are very similar to the ones obtained using the regional velocity model with relatively small differences in the focal mechanism, moment magnitude, or centroid depth. These estimates are also consistent with CAP solutions. This is particularly true for W-phase solutions obtained using a regional velocity model, which provides a slightly better agreement with centroid depths estimated for events 3 and 4 (cf. Table S2). This suggests minor improvements in W-phase depth estimates when using a regional model. W-phase and CAP solutions are systematically shallower than GCMT estimates with a depth difference ranging from 2 to 8 km. This is probably related to the depth bias noted by Hjörleifsdóttir and Ekström (2010) due to regional lateral heterogeneities.

5. Conclusion

We implement the W-phase algorithm at regional scale to rapidly characterize the source of moderate to large ($M_w \geq 5.0$) earthquakes in China and neighboring areas. Using data from dense regional seismic networks, this approach can automatically provide centroid moment tensor parameters within only 4 to 7 min after the earthquake origin time. To assess the accuracy of W-phase CMT estimates, our regional implementation is tested for all $M_w \geq 5.0$ events in the region from 2011 to 2015 along with the 2008 M_w = 7.9 Wenchuan and the 2011 M_w = 9.1 Tohoku earthquakes. The results demonstrate that regional W-phase CMT solutions are generally in good agreement with Global CMT solutions. One major limitation is the clipping of records at short distances, which prevent us from having reliable solutions in less than 4 min for large earthquakes. For such large events, our tests showed that solutions can still be obtained in 5 min by removing stations at very short epicentral distances depending on the preliminary magnitude of the earthquake. To provide faster estimates, we could also integrate other observations such as high-rate GPS providing direct measurements of near-field displacements. Our estimates can also be improved by incorporating regional 1-D velocity models. The regional W-phase implementation is now used in real time at the CENC to rapidly characterize the source of $M_w \geq 5.0$ earthquakes. Such rapid estimates can be used for various purposes such as tsunami warning and fast damage assessment that are essential to reduce the impact of earthquakes and initiate rapid emergency activities.

Acknowledgments
This study benefited from fruitful discussions with Hiroo Kanamori and Luis Rivera. The research described herein used seismological data provided by the Chinese Digital Seismic Networks and several international networks (GE, G, II, IU, JP, KR, KZ, and TW). The waveforms are accessed from the China Earthquake Networks Center, the Data Management Centre of the China National Seismic Network at the Institute of Geophysics, China Earthquake Administration (SEISDMC, doi: 10.7914/SN/CB, Zheng et al., 2010), and the Incorporated Research Institutions for Seismology (IRIS) Data Management System (DMS). The figures were plotted using the Generic Mapping Tools (GMT) software and Matplotlib Python module. The seismic waveforms were processed using the Seismic Analysis Code (SAC) software. This research was funded by the National Natural Science Foundation of China (grants 41390455, 41504046, and 41630210). We thank two anonymous reviewers and the editor (Yehuda Ben-Zion) for insightful comments that helped us to improve the manuscript.

References

Aki, K. (1967). Scaling law of seismic spectrum. *Journal of Geophysical Research*, *72*(4), 1217–1231. https://doi.org/10.1029/JZ072i004p01217
Bouchon, M. (2003). A review of the discrete wavenumber method. *Pure and Applied Geophysics*, *160*(3), 445–465. https://doi.org/10.1007/978-3-0348-8010-7_2

Dreger, D. S., Gee, L., Lombard, P., Murray, H. M., & Romanowicz, B. (2005). Rapid finite-source analysis and near-fault strong ground motions: Application to the 2003 M_w6. 5 San Simeon and 2004 M_W6.0 Parkfield earthquakes. *Seismological Research Letters*, *76*(1), 40–48. https://doi.org/10.1785/gssrl.76.1.40

Duputel, Z., Rivera, L., Kanamori, H., & Hayes, G. P. (2012). W phase source inversion for moderate to large earthquakes (1990–2010). *Geophysical Journal International*, *189*(2), 1125–1147. https://doi.org/10.1111/j.1365-246X.2012.05419.x

Duputel, Z., Rivera, L., Kanamori, H., Hayes, G. P., Hirsorn, B., & Weinstein, S. (2011). Real-time W phase inversions during the 2011 Tohoku-oki earthquake. *Earth, Planets and Space*, *63*(7), 535–539. https://doi.org/10.5047/eps.2011.05.032

Duputel, Z., Vergne, J., Rivera, L., Wittlinger, G., Farra, V., & Hetényi, G. (2016). The 2015 Gorkha earthquake: A large event illuminating the Main Himalayan Thrust fault. *Geophysical Research Letters*, *43*(6), 2517–2525. https://doi.org/10.1002/2016GL068083

Dziewonski, A. M., & Anderson, D. L. (1981). Preliminary reference Earth model. *Physics of the Earth and Planetary Interiors*, *25*(4), 297–356. https://doi.org/10.1016/0031-9201(81)90046-7

Dziewonski, A. M., Ekström, G., & Salganik, M. P. (1992). Centroid-moment tensor solutions for July–September 1991. *Physics of the Earth and Planetary Interiors*, *72*(1-2), 1–11. https://doi.org/10.1016/0031-9201(92)90044-V

Ekström, G., Nettles, M., & Dziewonski, A. M. (2012). The global CMT project 2004–2010: Centroid-moment tensors for 13,017 earthquakes. *Physics of the Earth and Planetary Interiors*, *200–201*, 1–9. https://doi.org/10.1016/j.pepi.2012.04.002

Hao, J. L., Ji, C., Wang, W. M., & Yao, Z. X. (2013). Rupture history of the 2013 M_w 6.6 Lushan earthquake constrained with local strong motion and teleseismic body and surface waves. *Geophysical Research Letters*, *40*(20), 5371–5376. https://doi.org/10.1002/2013GL056876

Hayes, G. P., Rivera, L., & Kanamori, H. (2009). Source inversion of the W-phase: Real-time implementation and extension to low magnitudes. *Seismological Research Letters*, *80*(5), 817–822. https://doi.org/10.1785/gssrl.80.5.817

Herrmann, R. B. (2013). Computer programs in seismology: An evolving tool for instruction and research. *Seismological Research Letters*, *84*(6), 1081–1088. https://doi.org/10.1785/0220110096

Hjörleifsdóttir, V., & Ekström, G. (2010). Effects of tree-dimensional Earth structure on CMT earthquake parameters. *Physics of the Earth and Planetary Interiors*, *29*(3), 139–151. https://doi.org/10.1007/s11589-016-0156-1

Kagan, Y. Y. (1991). 3-D rotation of double-couple earthquake sources. *Geophysical Journal International*, *106*(3), 709–716. https://doi.org/10.1111/j.1365-246X.1991.tb06343.x

Kanamori, H. (1993). W phase. *Geophysical Research Letters*, *20*(16), 1691–1694. https://doi.org/10.1029/93GL01883

Kanamori, H., & Given, J. W. (1981). Use of long-period surface waves for rapid determination of earthquake-source parameters. *Physics of the Earth and Planetary Interiors*, *27*(1), 8–31. https://doi.org/10.1016/0031-9201(81)90083-2

Kanamori, H., & Rivera, L. (2008a). Source inversion of W phase: Speeding up seismic tsunami warning. *Geophysical Journal International*, *175*(1), 222–238. https://doi.org/10.1111/j.1365-246X.2008.03887.x

Kanamori, H., & Rivera, L. (2008b). *Application of the W phase source inversion method to regional tsunami warning*. Paper presented at the Collection of Conference papers, International Conference on Tsunami Warning, Towards Safer Coastal Communities, Bali, Indonesia, (pp. 12–14).

Lee, S.-J., Huang, B.-S., Ando, M., Chiu, H.-C., & Wang, J.-H. (2011). Evidence of large scale repeating slip during the 2011 Tohoku-Oki earthquake. *Geophysical Research Letters*, *38*(19), L19306. https://doi.org/10.1029/2011GL049580

Parsons, T., Ji, C., & Kirby, E. (2008). Stress changes from the 2008 Wenchuan earthquake and increased hazard in the Sichuan basin. *Nature*, *454*(7203), 509–510. https://doi.org/10.1038/nature07177

Riquelme, S., Bravo, F., Melgar, D., Benavente, R., Geng, J., Barrientos, S., & Campos, J. (2016). W phase source inversion using high-rate regional GPS data for large earthquakes. *Geophysical Research Letters*, *43*(7), 3178–3185. https://doi.org/10.1002/2016GL068302

Rivera, L., & Kanamori, H. (2014). Diagnosing source geometrical complexity of large earthquakes. *Pure and Applied Geophysics*, *171*(10), 2819–2840. https://doi.org/10.1007/s00024-013-0769-4

Rivera, L., Kanamori, H., & Duputel, Z. (2011). W phase source inversion using the high-rate regional GPS data of the 2011 Tohoku-oki earthquake. AGU fall meeting 2011. https://doi.org/10.1590/S0120-41572011000300009

Shen, Z., Sun, J., Zhang, P., Wan, Y., Wang, M., Burgmann, R., … Wang, Q. L. (2009). Slip maxima at fault junctions and rupturing of barriers during the 2008 Wenchuan earthquake. *Nature Geoscience*, *2*(10), 718–724. https://doi.org/10.1038/ngeo636

Tsai, V. C., Hayes, G. P., & Duputel, Z. (2011). Constraints on the long-period moment-dip tradeoff for the Tohoku earthquake. *Geophysical Research Letters*, *38*, L00G17. https://doi.org/10.1029/2011GL049129

Wang, D., Becker, N. C., Walsh, D., Fryer, G. J., Weinstein, S. A., McCreery, C. S., … Shiro, B. (2012). Real-time forecasting of the April 11, 2012 Sumatra tsunami. *Geophysical Research Letters*, *39*, L19601. https://doi.org/10.1029/2012GL053081

Wang, Q., Qiao, X. J., Lan, Q. G., Freymueller, J. T., Yang, S. M., Xu, C. J., … Chen, G. (2011). Rupture of deep faults in the 2008 Wenchuan earthquake and uplift of the Longmen Shan. *Nature Geoscience*, *4*(9), 634–640. https://doi.org/10.1038/ngeo1210

Wang, W. M., Zhao, L. F., Li, J., & Yao, Z. X. (2008). Rupture process of the Ms 8.0 Wenchuan earthquake of Sichuan, China. *Chinese Journal of Geophysics*, *51*(5), 1403–1410.

Xu, X., Wen, X., Yu, G., Chen, G., Klinger, Y., Hubbard, J., & Shaw, J. H. (2009). Coseismic reverse- and oblique-slip surface faulting generated by the 2008 M_w 7.9 Wenchuan earthquake, China. *Geology*, *37*(6), 515–518. https://doi.org/10.1130/G25462A.1

Yue, H., Simons, M., Duputel, Z., Jiang, J., Fielding, E., Liang, C., … Samsonov, S. V. (2016). Depth varying rupture properties during the 2015 M_w 7.8 Gorkha (Nepal) earthquake. *Tectonophysics*, *714-715*, 44–54. https://doi.org/10.1016/j.tecto.2016.07.005

Zhao, L. S., & Helmberger, D. V. (1994). Source estimation from broadband regional seismograms. *Bulletin of the Seismological Society of America*, *84*(1), 91–104.

Zhao, X., Huang, Z. B., Fang, L. H., Li, Q., Zhao, B., & Miao, C. L. (2014). Kinematic characteristics of the source process of the Lushan, Sichuan Ms7.0 earthquake on 20 April 2013. *Chinese Journal of Geophysics*, *57*(2), 419–429. https://doi.org/10.6038/cjg20140208

Zheng, X. F., Yao, Z. X., Liang, J. H., & Zheng, J. (2010). The role played and opportunities provided by IGP DMC of China National Seismic Network in Wenchuan earthquake disaster relief and researches. *Bulletin of the Seismological Society of America*, *100*(5B), 2866–2872. https://doi.org/10.1785/0120090257